Design and Optimization of a Humidifier for an HDH System

by

Maximus Gladstone St. John

Submitted to the
Department of Mechanical Engineering
in Partial Fulfillment of the Requirements for the Degree of

Bachelor of Science in Mechanical Engineering

at the

Massachusetts Institute of Technology

June 2012
[September 2012]

Signiture of Author: _____
Department of Mechanical Engineering
May 23, 2012

Certified by: _____
John H. Lienhard V
Samuel C. Collins Professor of Mechanical Engineering
Thesis Supervisor

Accepted by: _____
John H. Lienhard V
Samuel C. Collins Professor of Mechanical Engineering
Undergraduate Officer

Design and Optimization of a Humidifier for an HDH System

by

Maximus Gladstone St. John

Submitted to the Department of Mechanical Engineering
on May 25, 2012 in Partial Fulfillment of the
Requirements for the Degree of

Bachelor of Science in Mechanical Engineering

ABSTRACT

Two billion people around the world do not access to clean drinking water. 98% of deaths caused by water related illness occur in the developing world. The humidification dehumidification desalination system currently being developed at the Lienhard Research Laboratory is a water treatment technology with low operational requirements that make it ideal for operation in the developing world. Researchers in the lab have just developed a novel design methodology for optimizing the performance of an HDH system based on thermal balancing, similar to the methodology used in heat exchanger design. An experimental pilot sized unit was built to test this methodology on a packed bed humidifier. Non-dimensional entropy generation was shown to have a minimum value for varied mass flow ratio as well as for varied water inlet temperature. At its optimal performance condition, the humidifier built for this thesis has a temperature pinch of 2.8 °C and an enthalpy pinch of 14.8 kJ/kg dry air. For the first time in literature, this thesis has experimentally shown that the balanced condition of HCR=1 corresponds to the condition of minimum entropy generation, validating the design methodology previously proposed at the Lienhard Lab.

Thesis Supervisor: John H. Lienhard V
Title: Samuel C. Collins Professor of Mechanical Engineering

Acknowledgements

This project has been a tremendous amount of work, and I do not hesitate to say that I could not have done it without a tremendous amount of help. To those that aided me in the completion of it, I am certainly indebted. Thank you for helping me to complete this project and for making it the successful experience that it was.

From his insights and assistance in the design, construction, and testing of the experimental plant to his advice on writing and proofreading of my thesis, Prakash Narayan Govindan has been an invaluable mentor and advisor to me throughout the entirety of this year long project. I would like to wholeheartedly thank him for all of this help.

Additionally, I would like to thank Victor Nevarez for all the time and effort he spent helping me build, design, and run the plant. Not only would the timely completion of this project have been impossible without his help, it would not have been nearly as much fun. Those 12-14 hour night long experiments would have been mind-numbingly tedious without his being there to help me record data.

Finally, I would like to thank Professor Lienhard and the Rohsenow Kendall Heat Transfer Lab for offering me the resources to turn this project the success that it became. Of all my experiences here at MIT, this project has been the most challenging and intellectually rewarding. The knowledge and experience I've gained as a result its completion is immeasurable.

Contents

List of Figures

Nomenclature

Symbols

c_p	Specific heat capacity at constant pressure (J/kg·K)
$\dot{C}$	Heat capacity rate (W/K)
$\dot{H}$	Total enthalpy rate (W)
h	Specific enthalpy (J/kg)
h_{fg}	Specific enthalpy of vaporization (J/kg)
HCR	Control volume based modified heat capacity rate ratio for HME devices (-)
$\dot{m}$	Mass flow rate (kg/s)
P	Absolute pressure (Pa)
$\dot{Q}$	Heat transfer rate (W)
R	Gas constant (J/kg·K)
s	Specific entropy (J/kg·K)
$\dot{S}_{gen}$	Entropy generation rate (W/K)
T	Temperature (°C)
T_{wb}	Wet bulb temperature (°C)

Greek

Δ	Change or difference
ε	Energy based effectiveness (-)
ϕ	Relative humidity (-)
Ψ	Enthalpy pinch (kJ/kg dry air)
Ψ_{TD}	Terminal enthalpy pinch

ω Absolute humidity

Subscripts

a Humid air

c Cold stream

da Dry air

h Hot stream

HE Heat exchanger

i Inlet

o Outlet

pw Pure water

sat Saturated

v Water vapor

w Seawater

1. Introduction

1.1 Motivation for HDH Optimization

More than 2 billion people around the world do not currently have access to a reliable source of potable water. A great majority of these people live in impoverished countries where lack of rainfall or lack of infrastructure required to purify rain and groundwater limit the availability of safe drinking water to levels below the 1,000 m^3/person-year deemed necessary to satisfy basic human needs [1]. By 2050, relative freshwater sufficiency will be 58%, while water scarcity, defined as the population living under the freshwater consumption limit above, will be 24%, as estimated by Population Action International [2-3]. Lack of fresh water forces people to drink water from untreated or contaminated sources. 90% of diarrheal illnesses in developing countries are attributed to the consumption of contaminated drinking water [4]. With cholera, typhoid fever, dysentery, and other diarrheal illnesses accounting for half the hospitalized people in the world, this is a very serious global health problem [5]. In addition to microorganism contaminants, water sources are often polluted by chemical contaminants like pesticides, fluoride, iron, arsenic, nitrates, and sodium. In India, 66 million people consume water with dangerous fluoride levels [6]. In West Bengal, over 300,000 people consume water with levels of arsenic above the permissible safe limit. Virtually every water source in Haiti, currently ranked last on the International Poverty Index for Western Countries, is contaminated by human waste [7]. Furthermore, in this water scarce country, the aquifer in its capital of Port-au-Prince is so low that the lack of pressure allows saltwater to seep in [8]. While these two countries are specific cases, water stress is a global problem. Figure 1-1 shows levels of water stress across the world. Red areas indicate water scarcity [9].

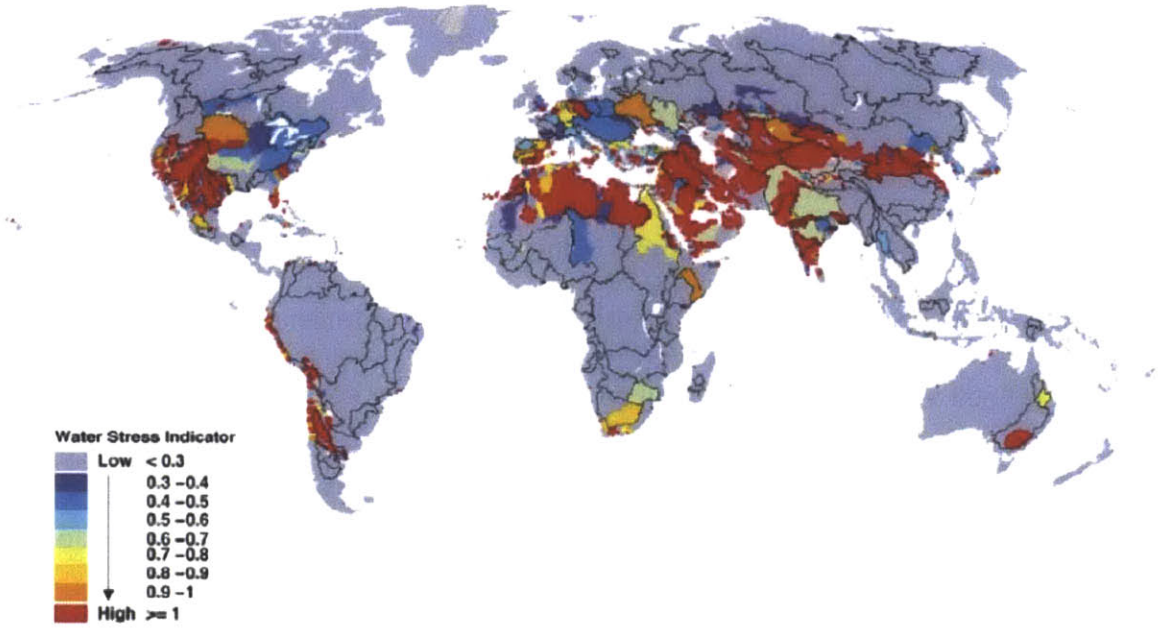

Figure 1-1: Global Water Stress [8]

Water treatment via desalination techniques is a prospective solution to this problem, with several techniques already established and many more currently being researched. Because the problems caused by water scarcity are most severe in developing world countries, the feasibility of small-scale desalination is severely limited by its capital cost and infrastructural requirements. Furthermore, a solution must be scalable to a wide range of contaminant varieties and concentrations. Humidification dehumidification is a very promising desalination technique that can also address the concerns listed above. This thesis will briefly compare desalination techniques, then describe the design, construction, and entropy minimization of a humidifier in an experimental HDH desalination plant.

1.2 Conventional Desalination Techniques

1.2.1 Reverse Osmosis

The most energy efficient type of desalination, and the most widely applied is Reverse Osmosis (RO). A typical seawater RO plant is built to supply several hundred thousand cubic meters of water per day at a cost of less than 1 US$/cubic meter. Experimentally, energy consumption as low as 3.5 kilowatt hour/cubic meter of treated water has been demonstrated for this type of system. Because of its high efficiency, it is widely used to produce fresh water wherever needed.

Osmosis is a process by which solvent molecules move through a semipermeable membrane from areas of lower to higher solute concentration. At equal pressures, a membrane separating saline from fresh water would allow the transport of water molecules from the latter to the former. The direction of this transport may be reversed by applying a positive pressure to the side with a higher solute concentration, forcing water molecules from the saline side to the pure water side. In an RO plant, like the one pictured in Figure 1-2, pressure is applied with a pump, and pressurized water is forced through RO membrane filters. Because the rate of transport through the membrane is a function of relative solute concentration, around 60% of the saltwater input to the system does not pass through the filters, and is used to transport excess salt from the system. Because RO membranes are sensitive to pH, oxidizers, organics, particulates, and other foulants, all input water, including the 60% that is not desalinated, must be pretreated. In addition to the energy cost required to run the pump, regular maintenance and filter replacement every 2-4 years, pretreatment costs are significant, especially when contaminant concentration is high [10]. While the operating cost of an RO plant can be much lower than for that of other methods of desalination, its capital cost per output can be much higher at smaller

scales, which is a considerable obstacle to solving the water problem in the developing world where capital investment is small. Most of the people who lack access to safe drinking water live in these low-income countries, and are frequently widely dispersed in rural areas, making water treatment at a small scale local level the only feasible solution. Further complicating the implementation of RO plants in addressing the world's water problems, is their heavy reliance on existing infrastructure. Not only is reliable power a necessity for a plant of this type, it needs a steady supply of costly RO filters, and a fully staffed engineer at all times to manage pretreatment, reduce scaling, and extend system life

Figure 1-2: Reverse Osmosis Plant [11]

1.2.2 Multistage Flash (MSF)

After RO, MSF is the second most commonly applied method of desalination, producing 40% of the world's desalinated water. MSF is commonly paired with fuel burning power plants, using low temperature steam extracted from the power plant's turbines as a heat source for this thermal desalination plant. [12]

In MSF, saline water is successively flashed in negatively pressurized chambers at descending negative pressures. The saline water first flows through cooling coils in the plant's condensers, recovering the energy released from the gas to water phase changes. Additional heat is added to the water, elevating it to a sub-boiling temperature before it is sprayed into an evaporator. In the presence of the reduced pressure, some water instantly boils off and separates from the liquid flow. This process is known as "flashing". Evaporated water condenses against the cooling coils, and the remaining liquid water is transferred to another evaporator operating at an even lower pressure. This flashing process is repeated several times at successively lower pressures. A schematic diagram of the fluid circuits involved in this process is shown below.

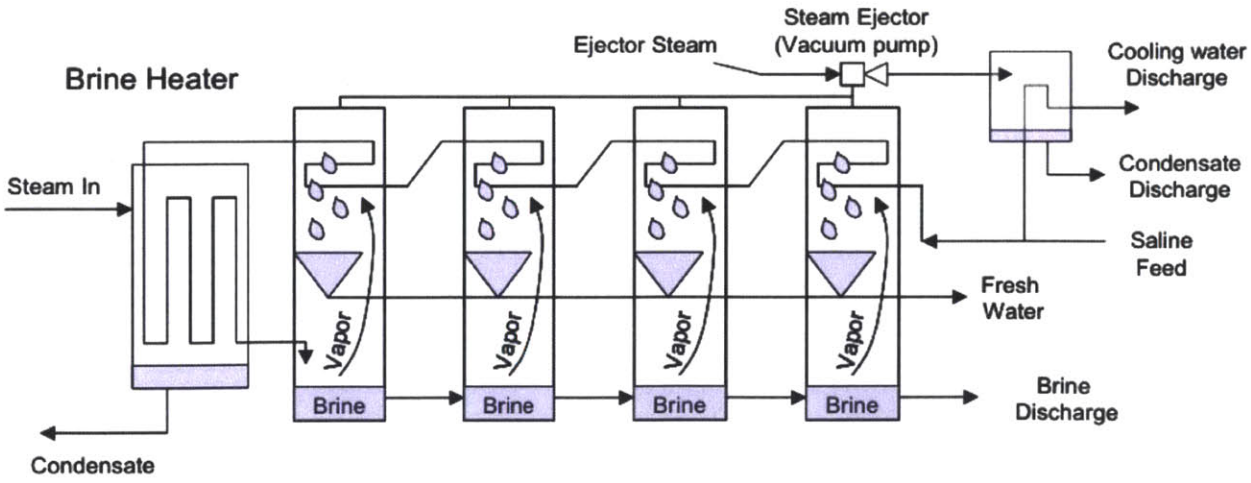

Figure 1-3: Schematic Diagram of a Multi-Stage Flash Desalination System [12]

The seawater flows through the condensers in order of ascending operating temperature. The flow absorbs the heat lost in the vapor-liquid phase change as the fresh water condenses, raising the temperature of the saline flow at each condenser. Running the coolant flow in ascending temperature order ensures that it is sufficiently cool to allow condensation, and reduces entropy generation in the condensers. Furthermore, the energy requirement is greatly reduced since a significant amount of energy is recovered from the condensers. The vaporization point of water is pressure, as well as temperature dependant, so the successively lower pressures of the evaporators allow the water to be repeatedly flashed with no additional thermal energy required.

Scaling inside the evaporators in these plants can be a serious problem. At higher temperatures, calcium, sulphate, and carbonate ions are less soluble in water. Since the seawater must be heated to around 90°C before it is flashed, these can form hard (and soft) scales that adhere to the walls of the pipes in the cooling coils, reducing heat transfer, and increasing the pressure required from the plant's pump. Furthermore, as water is vaporized in each successive stage, the solute concentration of the remaining water increases each time, increasing the chance of scaling. As a result, regular maintenance of these plants is required for continuous operation. These costs can be as high as 10-15% of the total cost of water production, and require trained personnel to undertake this task. For smaller plants on the scale of 1-100 m^3/day, the fixed cost of scale removal represents an even larger share of the water production cost.

1.2.3 Humidification Dehumidification

Humidification Dehumidification (HDH) is a new type of thermal desalination, that is currently under development by the Lienhard Research Group at MIT. Currently there are few

functional HDH plants in the world, but their benefits make them very well suited for a variety of markets.

An HDH system removes contaminants from water through the same mechanism as the water cycle. Water is heated by sunlight to a temperature greater than the air in its vicinity. Across this temperature differential, heat and mass are exchanged. The moist air is lifted high into the troposphere, where it cools, releasing its vapor as rain. The humidified air carries only the water vapor, so its condensate is pure.

As in an MSF plant, input seawater is used to cool the condensers, or dehumidifiers: a process which both heats the water in addition to cooling the moist air flow. The water is then heated and sprayed into a humidifier where it meets the cooled air from the dehumidifiers in a direct contact counter-flow. Heat and mass are transferred to the air stream, which carries its humidity to the dehumidifiers, and excess saline water is drained from the humidifier. In this thesis, the details of the operational performance of the humidifier are studied in great detail.

2. Design of an HDH System

2.1 Overview

HDH systems, like the plant built for this thesis, pictured in Figure 2-1, are classified according to three characteristics: energy source, heating type, and cycle configuration. Most of the energy required in an HDH system is needed in the form of heat. Therefore, an HDH system can be powered relatively cheaply by the combustion of low-grade waste fuels like corn husks or manure, both of which are widely available in developing world countries at extremely low cost. The thermal energy can either be used to heat the water or the air circuit before entry into the humidifier. For the purpose of heat recovery in the system, it is desirable that one of the fluid circuits be closed loop. Thus, cycle configuration is divided into: closed air, open water (CAOW); and closed water, open air (CWOA). For either of these configurations, air may be circulated through the system via natural convection or forced via a blower.

In a review of present HDH technology, Narayan et al. [13] found water heated, closed air open water circuit HDH plants with mass extraction loops to be the most energy efficient. Because system performance of an HDH plant is dominated by the performance of the dehumidifiers, the water production of a CWOA system is extremely dependent on the humidifier's capacity to lower temperature of the water provided for the dehumidifier's coolant flow. At optimal humidifier conditions, a closed water open air system can be more productive than the type built for this thesis; however, the sensitivity of the system to the humidifier's operating conditions makes the CWOA configuration undesirable. While mass extraction in an HDH system lies outside the scope of this thesis, the plant was designed to allow future experimental work in this area. Therefore, the system configuration of this plant follows the recommendations of Narayan et al.

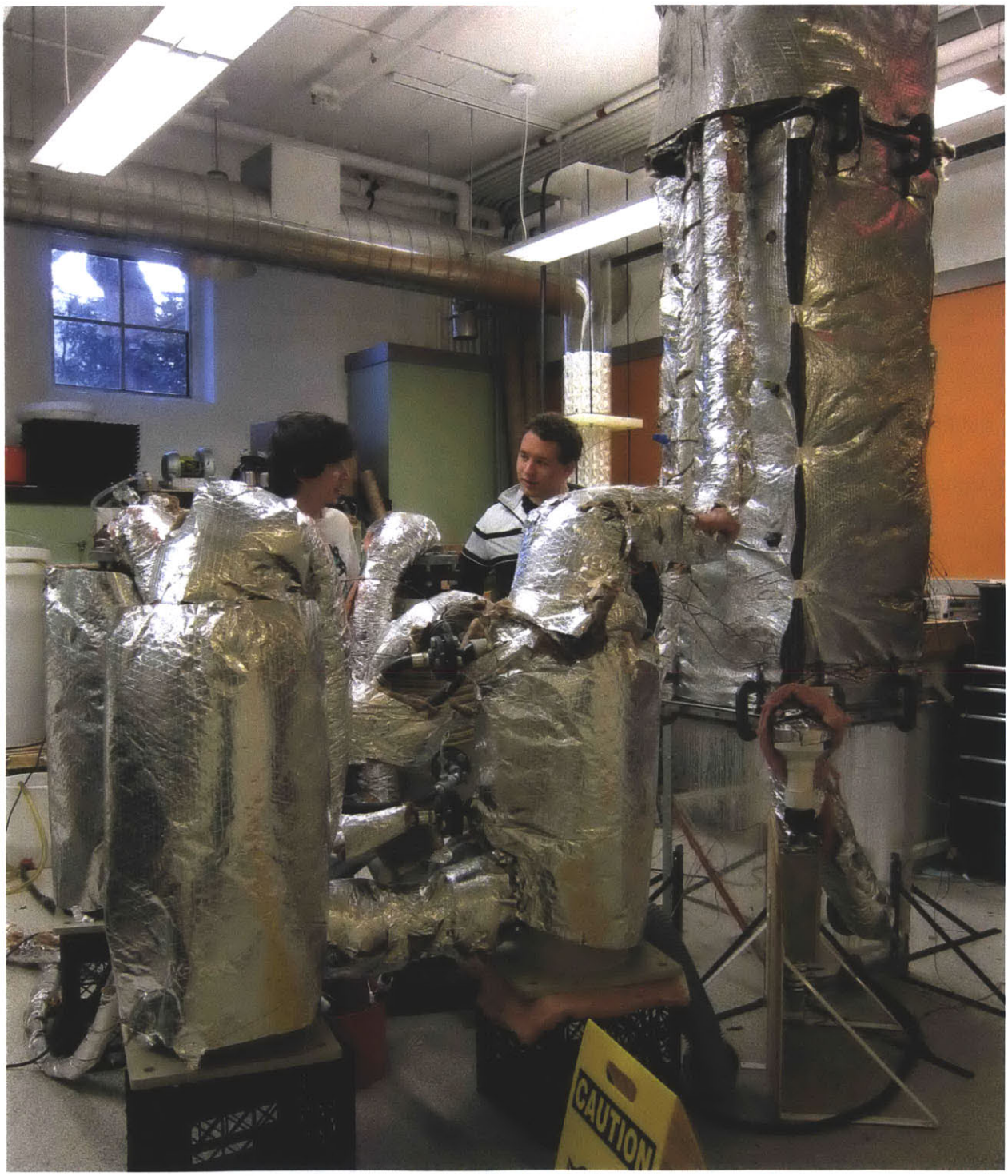

Figure 2-1: HDH Experimental Plant

2.2 Fluid Circuits

The air circuit is closed loop that carries water vapor from the humidifier to the dehumidifier, as shown in Figure 2-2. Air is driven by a blower through the bottom of the humidifier, where it meets the water circuit in a cross flow heat and mass exchange. Hot water evaporates into the air stream, raising the air's temperature and absolute humidity. Saturated moist air exiting the humidifier then enters the first dehumidifier, a heat exchanger chilled by a cold water flow. In this device, the temperature of the air is decreased, causing it to lose humidity as condensed water. Condensate flows out through the bottom of the dehumidifier, and is separated from the air by a condensate collection system. The air exiting the first dehumidifier is passed through three successively colder dehumidifiers, further decreasing the temperature and vapor content. After exiting the fourth dehumidifier, the air flow re-enters the blower.

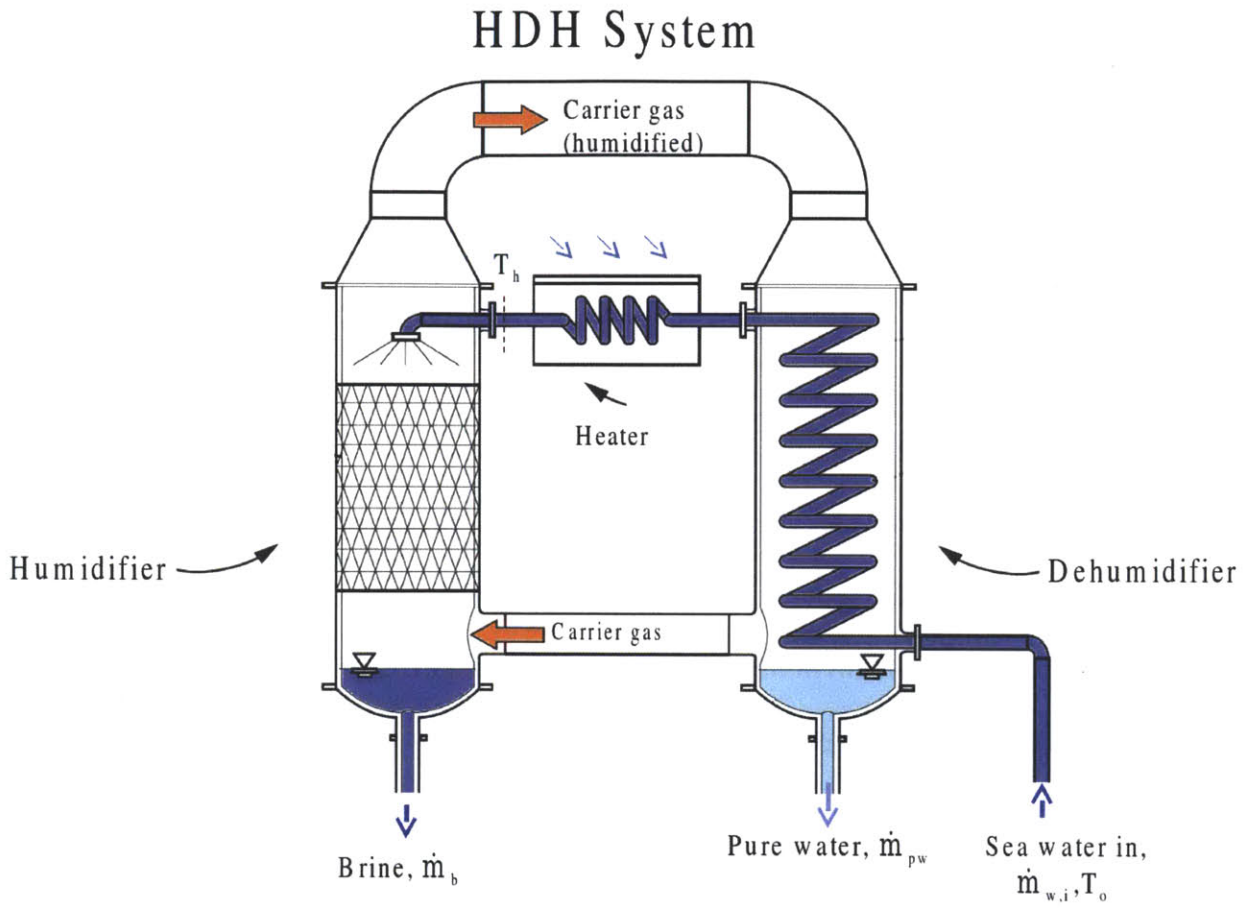

Figure 2-2: Schematic Diagram of an HDH System [14]

Chilled water from a tank is pumped through the dehumidifiers entering the fourth one first, flowing through the series in the opposite direction of the air flow. Heat transferred from the air flow and condensation elevates the temperature of the water through each dehumidifier. The water flow, preheated from the dehumidifiers, enters the water heater, where its temperature is increased significantly. Hot water exiting the heater is sprayed through the top of the dehumidifier. The contact with the air flow cools the water through heat transfer and evaporation. Some water enters the air flow as vapor, while the rest is pumped from the bottom of the humidifier back into the chilled water tank.

2.3 Dehumidifiers

This system used four tube plate dehumidifiers, an example of which is shown in Figure 2-3. Air flows through its center, and is cooled by water flowing through a series of plates in plane with the cross section. The plates each consist of 35 parallel 0.189'' ID tubes fed and drained by a two section header. Barriers at opposite corners of the headers divide it such that water can only flow from one side of the header to the other via the parallel tubes connecting them. Each plate is oriented 90° with respect to the previous one [15]. As shown in Figure 2-3, water enters the header through an inlet in one corner and flows through the parallel tubes to the opposite header section where it drains into the header below it. Since the headers separate the hot air flow from the external environment, head loss in these devices is reduced. This design combines the insulating benefits of a coaxial heat exchanger with the high heat transfer area of a standard shell and tube heat exchanger.

This experimental plant utilized polypropylene Calorplast Tube Plate heat exchangers built by Georg Fisher Piping Systems. The smooth surface afforded by polypropylene reduced the onset of fouling from salt deposits, and its high chemical inertness made the dehumidifiers virtually resistant to corrosion. While the experiments detailed in this thesis did not utilize saltwater, these characteristics were selected to allow future experimental work with contaminants. The series of four dehumidifiers used in the system had a total heat transfer area of 8 m^2 and a heat transfer coefficient of 140 $W/m^2 \cdot K$. The price of each unit was $3400. Dehumidifier performance dominates the system performance, so the high cost and intricate design of these components was well justified. Recently, however, a new low cost dehumidifier design has been invented by the Lienhard Research Group [17].

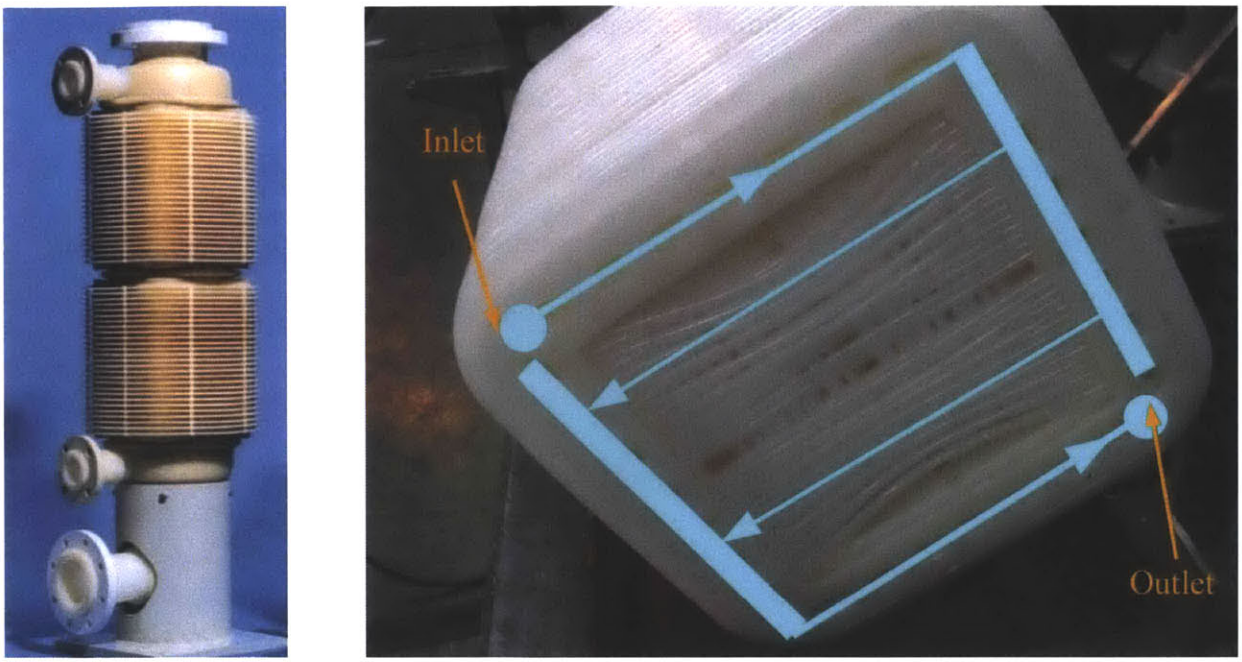

Figure 2-3: Calorplast Tube Plate Dehumidifier and Cross Section Flow Diagram [16]

2.4 Humidifier Design

2.4.1 Overview

The humidifier designed for this plant is shown as a CAD model in Figure 2-4. Air flows into the humidifier from the bottom, and exits through the top meeting the falling water in a counter-flow heat and mass exchange. Inside the humidifier are blocks of corrugated PVC sheets. These packed bed fills break the fall of the water and increase the surface area exposed to the airflow, which increases the evaporation. Air enters the humidifier at 100% relative humidity and exits conditions close to saturation. While the relative humidity is higher at the inlet, the temperature of the air at the outlet is much greater. The amount of vapor air can carry increases greatly with temperature, as shown in Figure 2-5. The moisture picked up by air in the humidifier constitutes the fresh water flow out of the system.

Three sections compose the humidifier: top, middle, and base. Each section is made of acrylic sheets of ¼ inch thickness. Along the vertical edges of the humidifier, the sheets are joined with aluminum angle brackets, fixed to the edges of the acrylic sheets with bolted joints. The angle brackets strengthen the structure of the humidifier, and eliminate water and air leaks through those junctions. The sectional design of the humidifier allows the disassembly of the humidifier required to replace or alter the fill configuration and reduces the cost of materials, as larger acrylic sheets are prohibitively expensive.

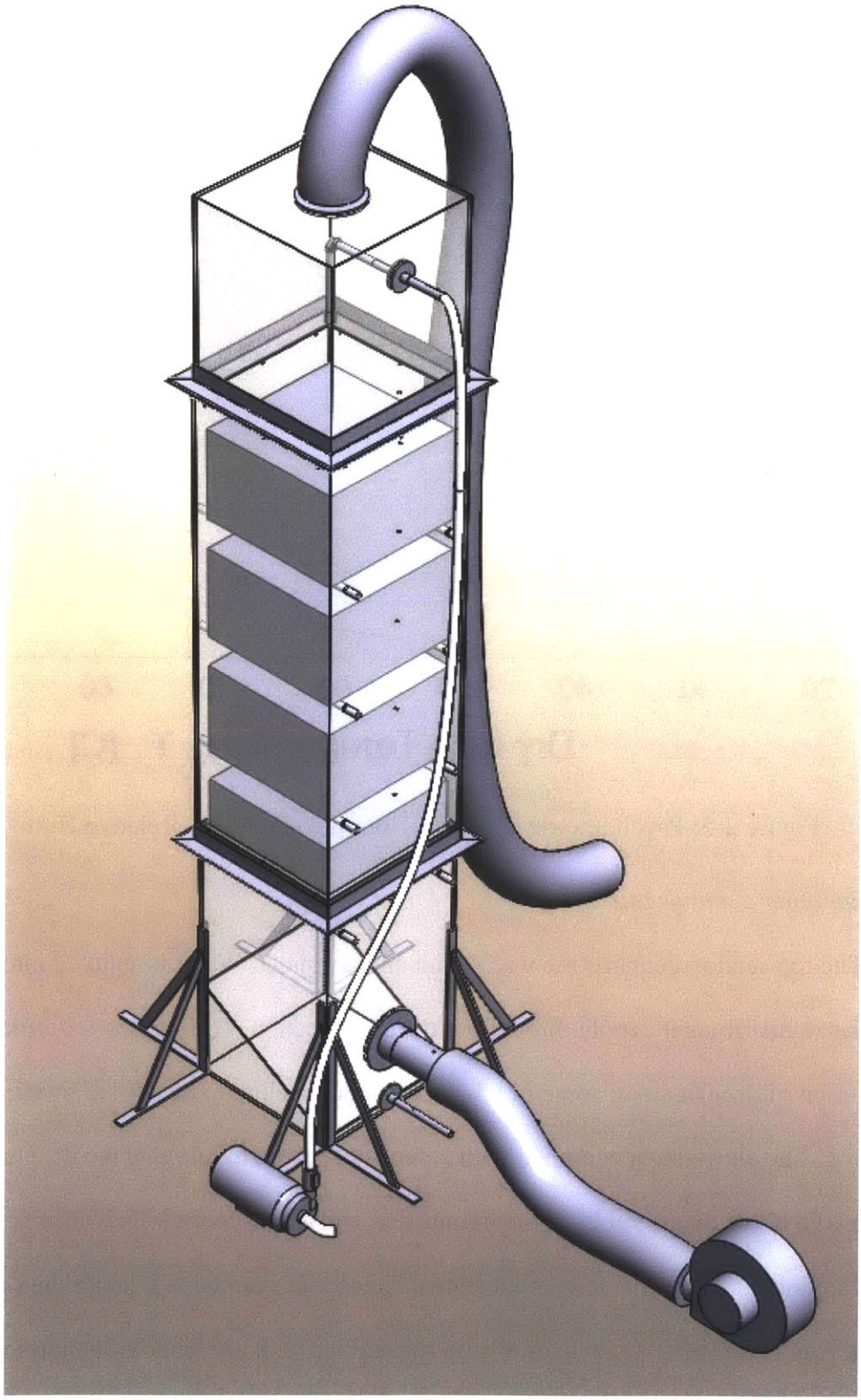

Figure 2-4: Humidifier CAD Diagram

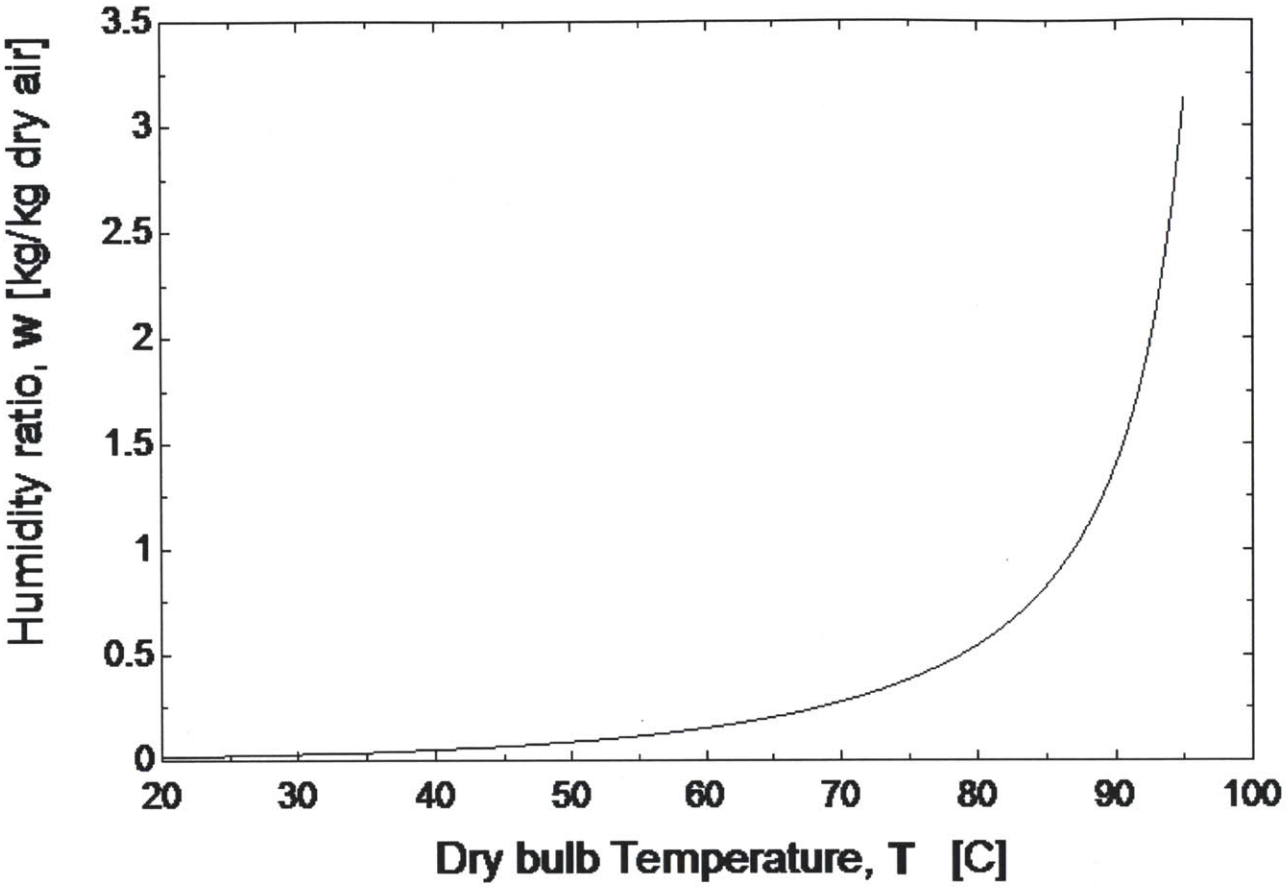

Figure 2-5: Psychometric Chart for Humid Air at 100% Relative Humidity

2.4.2 Humidifier Components

The top section contains the water inlet and air outlet. Water is sprayed into the humidifier to distribute it evenly throughout the cross section. The sprayer's nozzle creates a distribution of droplet sizes, some of which are small enough to be carried by the air in suspension. The air outlet is equipped with a demister screen to mitigate the droplet flow carried by the air. To allow disassembly of the humidifier, and access to the fills within it, the humidifier sections are joined with separable connections. All sections are joined via flanged connections, and the top and bottom sections feature a lip that extends into the middle section for added support. Flanges are clamped tightly together via eight c-clamps per junction to eliminate air

leaks through the flanges.

The middle section contains the packed bed heat transfer fills, as shown in Figure 2-6. The uppermost fill is positioned directly under the sprayer nozzle such that the spray cone intersects the top of the fill before it can reach the wall, stopping the water from running down the walls. Water running down the walls falls much faster than water falling through the fills, which reduces the time it can effectively transfer heat and mass to the air. Furthermore, it contributes to heat loss in the humidifier. Water has both a higher heat capacity and higher thermal conductivity than air, so water at the walls of the humidifier increases heat loss. The fills are supported by aluminum rods which can be inserted at three points in the middle section and at one point in the base section to allow a variety of fill volumes and configurations.

At the bottom junction, a water diverting skirt prevents leakage through the narrow gap between the walls of the middle second and the extending lip of the bottom section, as shown in Figure 2-7. Air enters through an inlet duct in the base, positioned six inches above the water outlet line in the base section, as shown in the CAD drawing in Figure 2-4. An angled plate guides water to this drainage line. Since the humidifier is tall, eight support brackets are fixed to the base to widen the footprint of the humidifier and reduce the risk of tipping.

Figure 2-6: Heat Transfer Fills in the Middle Section

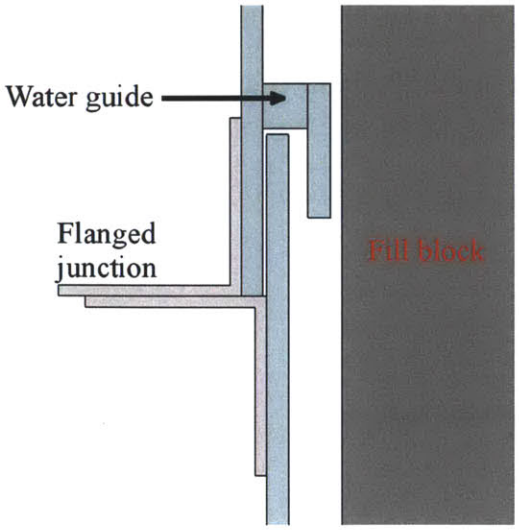

Figure 2-7: Diagram of Water Diverting Skirt

2.4.3 Design constraints

The dimensions of the humidifier design were driven by the requirements for the total fill volume and its cross sectional area. The effectiveness and Merkel number depend on these geometric constraints. Sharqawy et al. proposed a model for predicting the performance of cooling tower for the purpose of desalination [18]. The model iteratively solves energy and mass balances on moist air, water vapor, sea water and salts contained in the seawater to predict Merkel number and effectiveness of a humidifier. Using desired temperature inlets and outlets, and humidity ratios of saturated air at those temperatures, the cross sectional area and fill volume were chosen to produce the desired Merkel numbers and effectivenesses [18]. These values are given in the diagram in Figure 2-8.

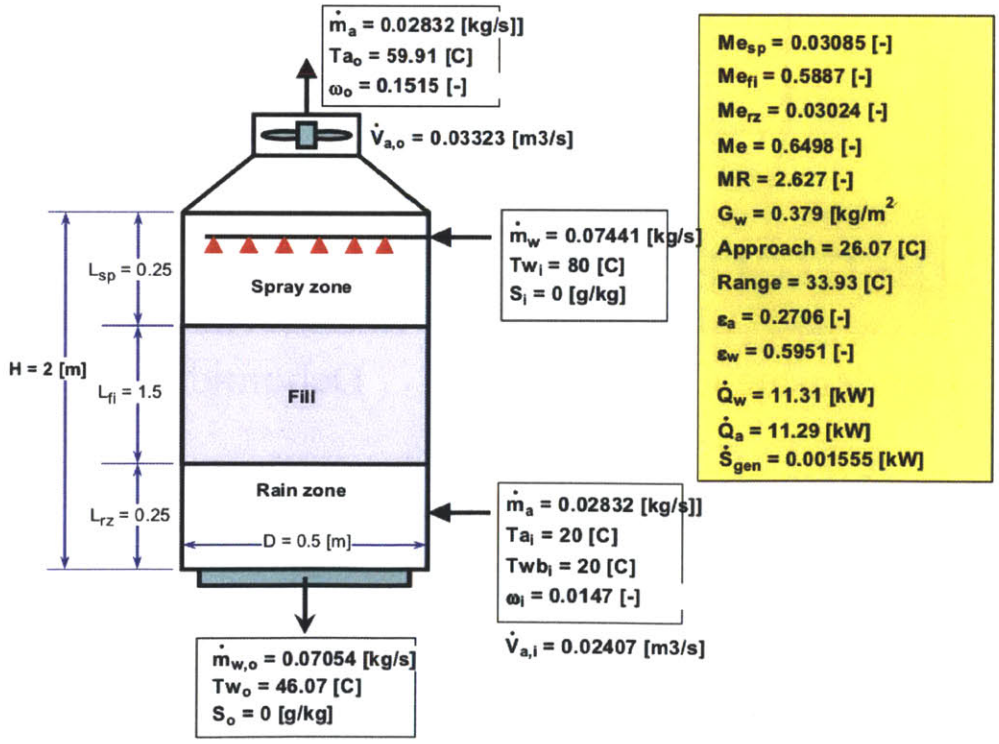

Figure 2-8: Design Points for the Humidifier [19]

2.5 Condensate collection

Water condensed in the dehumidifiers exits with the air stream. The condensate is separated from the airflow and drained into a condensate reservoir. Figure 2-9 depicts a schematic of the condensate collection system.

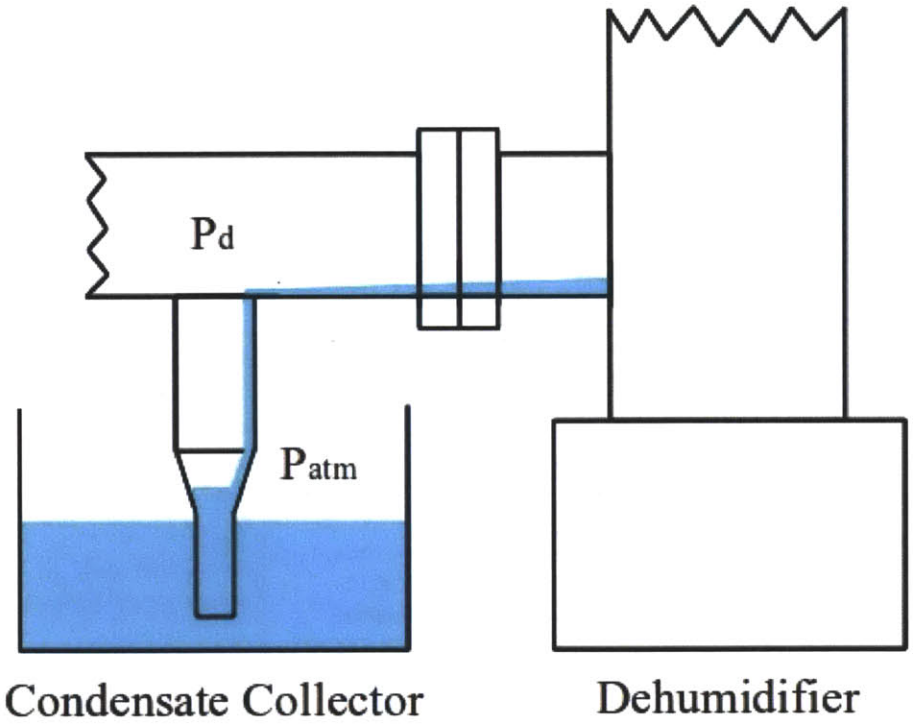

Figure 2-9: Condensate Collection Diagram.

Each dehumidifier operates at a different pressure spanning atmospheric, due to the pressure rise across the blower and pressure drops throughout the system. Raising the dehumidifiers above the level of the reservoir was required to prevent backflow of condensate into those operating slightly below atmospheric, and the drain line was submerged to prevent air flow through the drain line at those operating above atmospheric pressure.

2.6 Blower selection

Air moving units fall into three categories: compressors, blowers, and fans. The difference between them is based on pressure rise across the unit, and flowrate through it. Compressors operate at high pressures, typically with low flow rates, and fans operate with almost no pressure rise with a wide range of flow rates. Blowers fill the gap between fans and compressors. The system required a maximum flow rate of 16.67 standard liters per second (60 m^3/hour), across a pressure drop on the order of 1 kPa (10 mbar). Shown below is the pressure vs. air flow chart of the Gast R2303A blower chosen for this system. As can be seen from this figure, this blower meets the pressure and flow rate requirements.

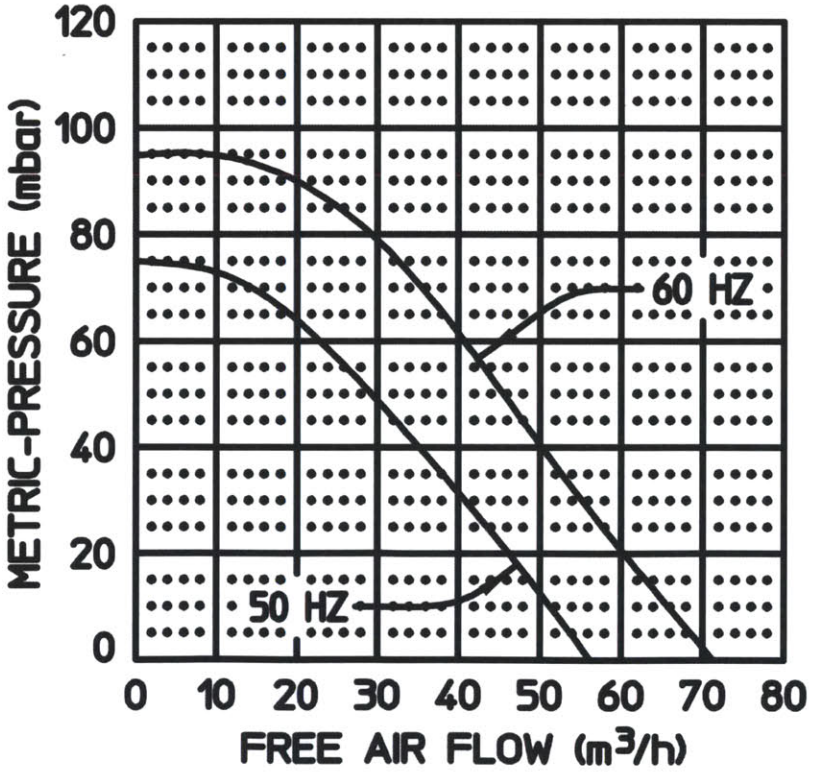

Figure 2-10: Pressure vs. Flow Rate Chart for the Gast R2303A Blower [20]

To examine the effect of different flow rates on the system, it was necessary to vary the power of the blower. While the option of throttling the airflow with a valve was explored, fine tuning of airflow proved to be difficult via this method. The blower chosen was driven by a ⅓ hp AC motor requiring 3 phase 240V current. The speed of an AC motor is directly proportional to the frequency of the current driving it, so varying the flow rate was simply a matter of controlling electric frequency via a frequency modulator.

Another consideration relevant to blower selection was the blowers ability to handle moisture. Air exiting the humidifier is saturated at 100% relative humidity. Since the dehumidifiers remove vapor content by cooling the air, the air entering the blower is still at 100% relative humidity, albeit at a lower absolute humidity. Water condenses from saturated air due to both temperature drops and pressure rises, thus the pressure at the boundary between the blower's turbine blades and the air causes condensation to form inside the blower. While many blowers utilize the air stream in directly cooling the motor, this was not acceptable in the design of this system as condensed water in the airflow could short the motor.

2.7 Pump selection

Pump selection was driven by flow rate and pressure drop requirements of 2.84 liters per minute and 2.6 kPa, respectively. Given these requirements, a centrifugal pump was the obvious choice. The pump selected for this system was a Taco 0011 circulator pump. The pressure vs. flow rate for the selected pump is shown on the following page.

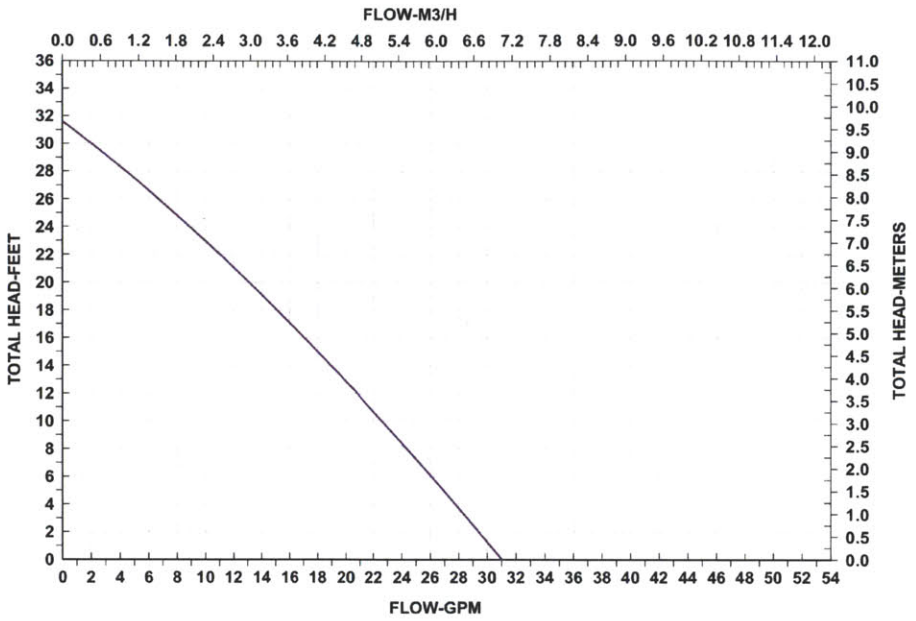

Figure 2-11: Pressure vs. Flow Rate of the Taco 0011 Centrifugal Circulator Pump [21]

2.8 Heater selection

To bring the system to a steady state as quickly as possible, the heater was required to raise the temperature of the water from that of the chilled water tank (20 °C), to a target temperature of 80 °C. The power required for temperature difference at a water flow rate of 2.84 liters per minute is easily calculated using equation 1 below.

$$\dot{Q}_{heater} = \dot{m}_w c_{p,w}(T_{w,in} - T_{w,o}) \tag{1}$$

For these conditions, the required power is nearly 12 kW. The heater selected for this system was a 12.7 kW Rheem EcoSense tankless electric water heater designed for domestic use. To safeguard against boiling in the pipes, the heater was equipped with a sensor that limited the water outlet temperature to a maximum of 150 °F. Since higher temperatures were required for the experiments in this thesis, this sensor was removed. A thermocouple was added immediately

after the heater, so the temperature could be monitored.

2.9 Future Design Recommendations

The HDH system built for this thesis was extremely effective; however, some aspects of its design made its construction unnecessarily difficult. Furthermore, some issues were discovered during the course of testing that did not affect the plant's thermal performance, but would have been a substantial hazard for a plant designed for the purpose of treating water.

The rectangular shape of the humidifier required numerous junctions between acrylic sheets. Each of these junctions had a significant risk of leakage, so this proved to be a significant design flaw. This was particularly problematic in the base since it constantly held at least three inches of water during operation. The weight of the water in the base caused significant stress on the seams between the acrylic plates, opening gaps between them, and causing water leakage. A great deal of sealant and a tremendous amount of time was required to fix the leaks at the seams. Additionally, acrylic sheets should not have been used to provide the structure of the humidifier. The strength and durability of the subsections, which took constant abuse during the disassembly and reassembly required to replace the fills, could have been greatly improved with the use of an underlying structural frame. In absence of such a frame, large forces on the seams joining the plates resulted in deformations that destroyed the seals that made the humidifier air and water tight. Furthermore, the consequences of fracturing of any of the sheets would been tremendous, requiring the refabrication of an entire subsection. Another solution to this problem is the tubular humidifier design used by Huang [22]. Each tubular section only requires two junctions, rather than the six required by a square cross section, eliminating many points of stress concentration and possible leakage.

While the sprayer nozzle used in this system was well suited for the testing of thermodynamic properties of the humidifier, it produced a distribution of droplet sizes, some which were sufficiently small to be carried directly by the air flow into the dehumidifiers. In a functional HDH plant, this is not acceptable, as the carried droplets never undergo a phase change, and are not purified.

3. Terminology

3.1 Heat Exchanger Terminology

Widely used methods for evaluating the entropy generation and exit conditions of heat exchangers have existed for almost 60 years [23]. Since heat and mass exchanger (HME) parameters described later in this section are analogous to those used in heat exchanger design, a brief overview heat exchanger parameters is given below.

The effectiveness for a counterflow heat exchanger, defined by equation 2, is used in the $\epsilon - NTU$ method of calculating exit temperatures and heat transfer. Effectiveness compares actual performance to ideal performance, so it can also be used as a metric to compare the performance of heat exchangers [24].

$$\varepsilon_{HE} = \frac{\dot{C}_h(T_{h,in} - T_{h,out})}{\dot{C}_{\min}(T_{h,in} - T_{c,in})} = \frac{\dot{C}_c(T_{c,out} - T_{c,in})}{\dot{C}_{\min}(T_{h,in} - T_{c,in})} \tag{2}$$

In the equation above, $C_{\min}$ is the lower of the two heat capacity rates. The lower heat capacity rate defines the limit of the heat transfer for a heat exchanger of this type.

The ratio of heat capacities, or heat capacity rate ratio (HCR), is defined as

$$HCR = \frac{C_c}{C_h} \tag{3}$$

Entropy generation is defined by the Second Law. The assumptions of incompressibility and negligible pressure drop result in equation 3.

$$\dot{S}_{gen} = \dot{m}_c c_{p,c} \ln\left(\frac{T_{2,c}}{T_{1,c}}\right) + \dot{m}_h c_{p,h} \ln\left(\frac{T_{1,h}}{T_{2,h}}\right) \geq 0 \tag{4}$$

Entropy generation is non-dimensionalized by dividing by the smaller heat capacity rate, so non-dimensional entropy generation is defined differently in two different cases.

Case I. $\dot{C}_c < \dot{C}_h$:

$$\frac{\dot{S}_{gen}}{\dot{C}_c} = \frac{1}{HCR} \cdot \ln\left\{1 - \varepsilon \cdot HCR\left(1 - \frac{T_{1,c}}{T_{2,h}}\right)\right\} + \ln\left\{1 + \varepsilon \cdot \left(\frac{T_{1,c}}{T_{2,c}} - 1\right)\right\} \quad (5)$$

Case II. $\dot{C}_c > \dot{C}_h$.

$$\frac{\dot{S}_{gen}}{\dot{C}_h} = HCR \cdot \ln\left\{1 + \frac{1}{HCR} \cdot \varepsilon\left(\frac{T_{2,h}}{T_{1,c}} - 1\right)\right\} + \ln\left\{1 - \varepsilon \cdot \left(1 - \frac{T_{1,c}}{T_{2,h}}\right)\right\} \quad (6)$$

From the First Law, when the heat capacity rate ratio is equal to 1, the temperature changes in the direction of the flow for the two streams is equal and the stream to stream temperature difference is constant throughout heat exchanger. The condition of HCR=1 defines a 'balanced' heat exchanger. From the conditional equation above, it can easily be shown that this condition minimizes non-dimensional entropy generation

3.2 Effectiveness of a Humidifier

An analogous effectiveness for HMEs is more difficult to characterize since the change in enthalpy of the air flow is a function of humidity as well as temperature. Furthermore, the effectiveness of enthalpy flows does not fully characterize the system, since the exiting air can have a range of humidity ratios and temperatures all corresponding to the same enthalpy rate. This latter problem is addressed by leaving exit humidity as a design constraint. To address the former problem, Narayan et. al [25] defines effectiveness in terms of the difference in enthalpy rate, as shown in equation 5 below.

$$\varepsilon = \frac{\Delta \dot{H}}{\Delta \dot{H}_{max}} \quad (7)$$

The choice of fluid stream for which effectiveness is evaluated is governed by lower heat capacity rate.

$$\varepsilon = \begin{cases} \dfrac{\dot{m}_{w,i}h_{w,i} - \dot{m}_{w,o}h_{w,o})}{\dot{m}_{w,i}h_{w,i} - \dot{m}_{w,o}h_{w,o}^{ideal}} & \text{If } \Delta\dot{H}_{\max,w} < \Delta\dot{H}_{\max,a} \\ \dfrac{\dot{m}_{da}(h_{a,o} - h_{a,i})}{\dot{m}_{da}(h_{a,o}^{ideal} - h_{a,i})} & \text{If } \Delta\dot{H}_{\max,w} > \Delta\dot{H}_{\max,a} \end{cases} \quad (8)$$

For the former case, the heat capacity rate of the water is insufficient to raise the temperature of the air to the water's inlet temperature, so in an infinitely sized HME, it follows that, at its outlet, the water flow would reach the temperature of the air inlet, thus these conditions are used to bound effectiveness in this case. However, if the heat capacity rate of the air is smaller, it will be insufficient to raise the water outlet temperature to the air inlet temperature, thus the ideal condition is evaluated for the other flow.

The above definition of effectiveness varies from 0 to a maximum value. To establish a definition of effectiveness analogous to that of heat exchangers, Narayan et al. [25] divide this definition by its maximum value, so as to vary it from 0 to 1. The maximum effectiveness is determined by one of two conditions, depending on the minimum terminal temperature difference. When the outlet air temperature does not reach the water inlet temperature, the maximum effectiveness is bounded by the Second Law ($\dot{S}_{gen} = 0$). This condition results in a high relative humidity and corresponds to the horizontal segments of the curves plotted in Figure 3-1. If the air outlet temperature does reach the air inlet, entropy is generated, and this condition bounds the maximum effectiveness. Enthalpy varies almost linearly with relative humidity for this condition, resulting in the positively sloped segment in Figure 3-1.

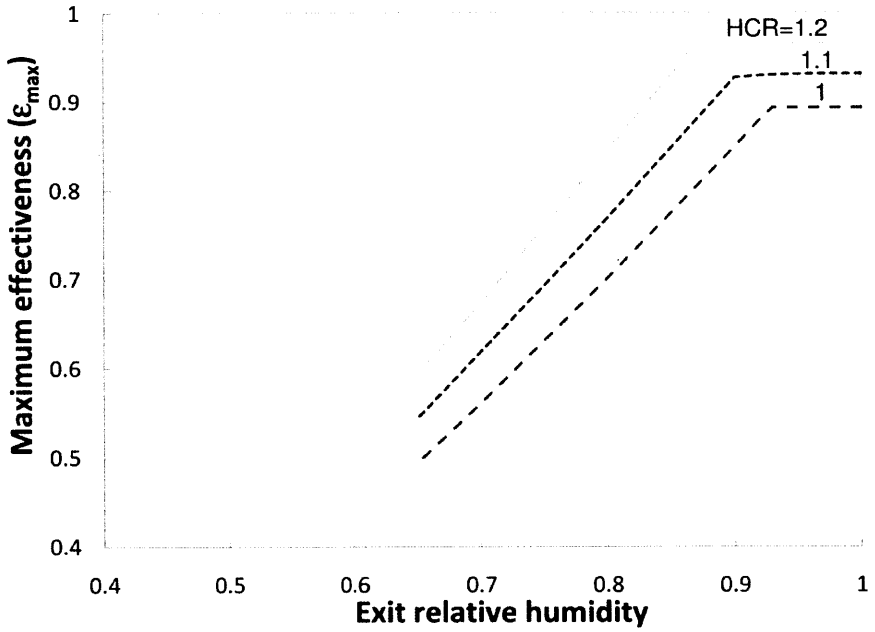

Figure 3-1: Exit Relative Humidity of a Humidifier vs. Maximum Effectiveness: $T_{w,i} = 55^oC$; $T_{a,i} = 34^oC; \phi_i = 100; P = P_{atm}$[25]

3.3 Modified Heat Capacity Rate Ratio

The heat capacity rate ratio of a HME cannot be defined as simply as it is for heat exchangers. The mass flow rate of the water is greater at its inlet than at its outlet, as some part of it is transferred to the air flow as humidity. Furthermore, the heat capacity of air is greatly dependent on relative humidity. Water is transferred to the air flow during its path through the humidifier, so outlet humidity, and therefore heat capacity rate as well, is greater at the outlet than at the inlet for the air flow. To address this problem, Narayan, et al. [25] defines heat capacity rate in terms of enthalpy changes.

For an infinite counterflow heat exchanger, the outlet temperature of either flow reaches the inlet temperature of the other. Thus, the heat capacity rate ratio for a heat exchanger can be rewritten as

$$HCR = \frac{\dot{C}_c}{\dot{C}_h} = \frac{\Delta \dot{H}_{\max,c}}{\Delta \dot{H}_{\max,h}} \tag{9}$$

since

$$\Delta \dot{H}_{\max} = \dot{m} c_p (T_{h,i} - T_{c,i}) \tag{10}$$

for either flow.

Likewise, HCR can be defined for a HME as,

$$HCR = \frac{\Delta \dot{H}_{\max,c}}{\Delta \dot{H}_{\max,h}} \tag{11}$$

3.4 Non-dimensional Entropy Generation

For heat exchangers, a non-dimensional entropy generation was defined for which the balanced condition minimized entropy generation. Likewise, entropy generation can be defined and non-dimensionalized for an HME.

Accounting for the change in mass flow rate of the water, due to evaporation Narayan et al. [26] defines entropy generation in a humidifier as,

$$\dot{S}_{gen} = \dot{m}_{w,o} s_{w,o} - \dot{m}_{w,i} s_{w,i} + \dot{m}_{da}(s_{a,o} - s_{a,i}) \tag{12}$$

The above equation is nondimensionalized by dividing it by the minimum heat capacity rate. Thus, there are two cases.

Case I. $\dot{H}_{\max,w} < \dot{H}_{\max,a}$:

$$\frac{\dot{S}_{gen}}{(\dot{m} \cdot c_p)_{\min}} = \frac{\dot{S}_{gen}}{(\widehat{\dot{m}_w} \cdot c_{p,w})} \tag{13}$$

Case II. $\dot{H}_{\max,w} > \dot{H}_{\max,a}$:

$$\frac{\dot{S}_{gen}}{(\dot{m} \cdot c_p)_{\min}} = \frac{\dot{S}_{gen}}{(\widehat{\dot{m}_w} \cdot c_{p,w} \cdot HCR)} \tag{14}$$

where,

$$\widehat{\dot{m}_w} \approx \frac{\dot{m}_{w,i} + \dot{m}_{w,o}}{2} \tag{15}$$

and $\widehat{(\dot{m}_w \cdot c_{p,w})} \cdot HCR$ is an approximation for the moist air heat capacity. In the next section, experimental proof will be given for the minimization of non-dimensional entropy generation under the balanced condition of HCR=1.

3.5 Enthalpy Pinch

While effectiveness is a suitable metric for evaluating HMEs with single inlets and outlets for both air and water, it only considers the terminal conditions of the device. For an HDH system with mass extraction lines between points the dehumidifiers and locations on the humidifier, the humidifier effectively has many inlets. Narayan et al. have proposed a method analogous to temperature pinch for evaluating HMEs of this type.

Temperature pinch is a useful parameter in analyzing heat exchanger devices, but once again, cannot be applied accurately to HMEs since the heat capacity of the airflow varies throughout the humidifier. Thus, the point of minimum local entropy generation may not be at the temperature pinch. In examining this phenomenon, consider Figure 3-2, on the following page.

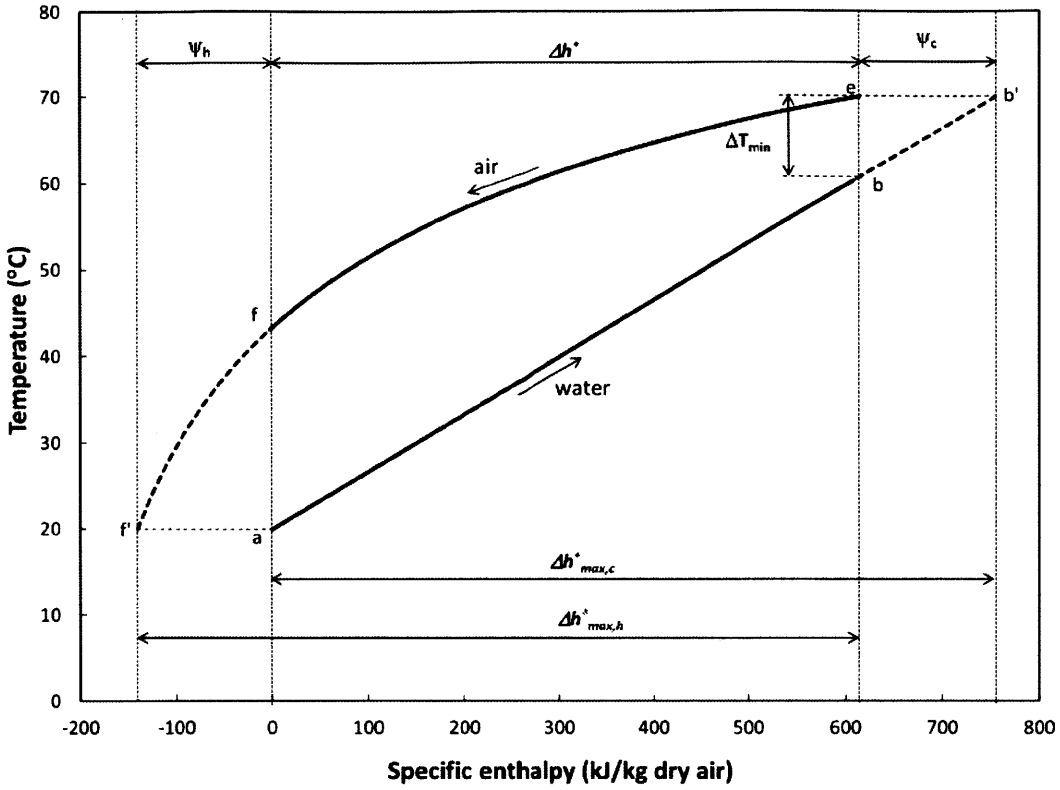

Figure 3-2: Temperature vs. Specific Enthalpy of Air and Water in a Dehumidifier [27]

The enthalpy of the water and air in a dehumidifier are plotted against temperature. Through recovery of the latent heat of condensation and heat transfer from the hotter air stream, water gains enthalpy linearly with temperature from a to b in the figure above because its heat capacity is essentially constant. As air travels through the dehumidifier, it transfers enthalpy to coolant flow, decreasing in temperature and enthalpy along the e to f path. For a dehumidifier of infinite size, air and water paths extend along the f to f' and b to b' lines respectively. Enthalpy not transferred between the two streams gets lost. The amount of enthalpy lost this way determines the effectiveness of the dehumidifier. Enthalpy lost from the air and water streams due to the finite size of the humidifier are denoted as Ψ_h and Ψ_c respectively in the figure above. Thus effectiveness can be defined in terms of the lost enthalpy.

$$\varepsilon = \frac{\Delta \dot{H}}{\Delta \dot{H} + \Psi_{TD}} \tag{16}$$

For,

$$\Psi_{TD} = \min(\Psi_c, \Psi_h) \tag{17}$$

For a dehumidifier with a single inlets and outlets for air and water the lowest stream to stream enthalpy difference will occur at one of the terminal points. However, for a humidifier, where the air curve lies below the water curve as shown in Figure 3-3, the lowest enthalpy difference can occur anyplace between those points depending on the mass flow ratio.

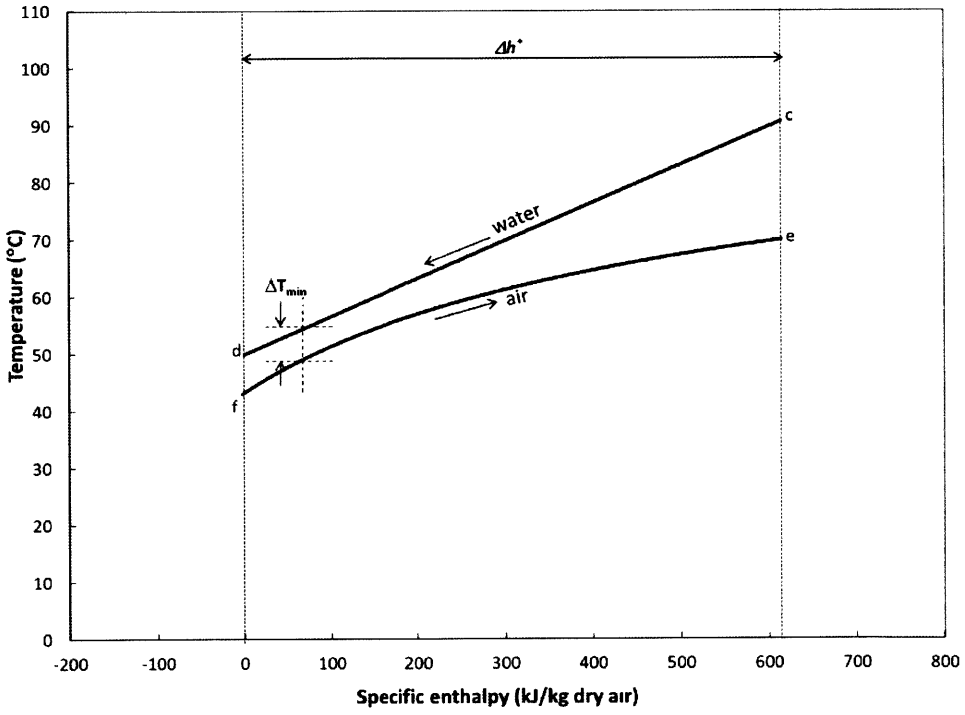

Figure 3-3: Temperature vs. Specific Enthalpy of Air and Water in a Humidifier [27]

Thus, to characterize a humidifier with an stream to stream enthalpy difference at the point of lowest entropy generation, the enthalpy pinch must be defined locally as

$$\Psi = \min_{local}(\Delta h_{max} - \Delta h) \tag{18}$$

4. Results

4.1 Effect of water inlet temperature

Figure 4-1 shows water inlet temperature to the humidifier plotted against energy effectiveness and modified heat capacity rate ratio for a mass flow ratio of 2.9, and a humidifier fill volume of 4 blocks (0.27 m^3). The HCRh in each trial, except that with water inlet temperature of 53.5 °C, is greater than or equal to 1. For this range, effectiveness is defined by the change in enthalpy rate of the water stream. Since the temperature of the air inlet was held constant, and the enthalpy of the water at its outlet is an increasing function of water inlet temperature, effectiveness also increases with the water inlet temperature for this range.

Below this range, effectiveness is defined by the change in enthalpy rate of the air flow. At a fixed relative humidity, the enthalpy of moist air is an increasing function of temperature that grows faster at higher temperature values. Since the ideal temperature of the air outlet is greater than its actual value, effectiveness decreases with temperature for this range. Therefore, an inlet temperature for which energy effectiveness is minimized must exist, and that inlet temperature must correspond to a HCRh value of to 1. The results plotted in Figure 4-1 support this conclusion.

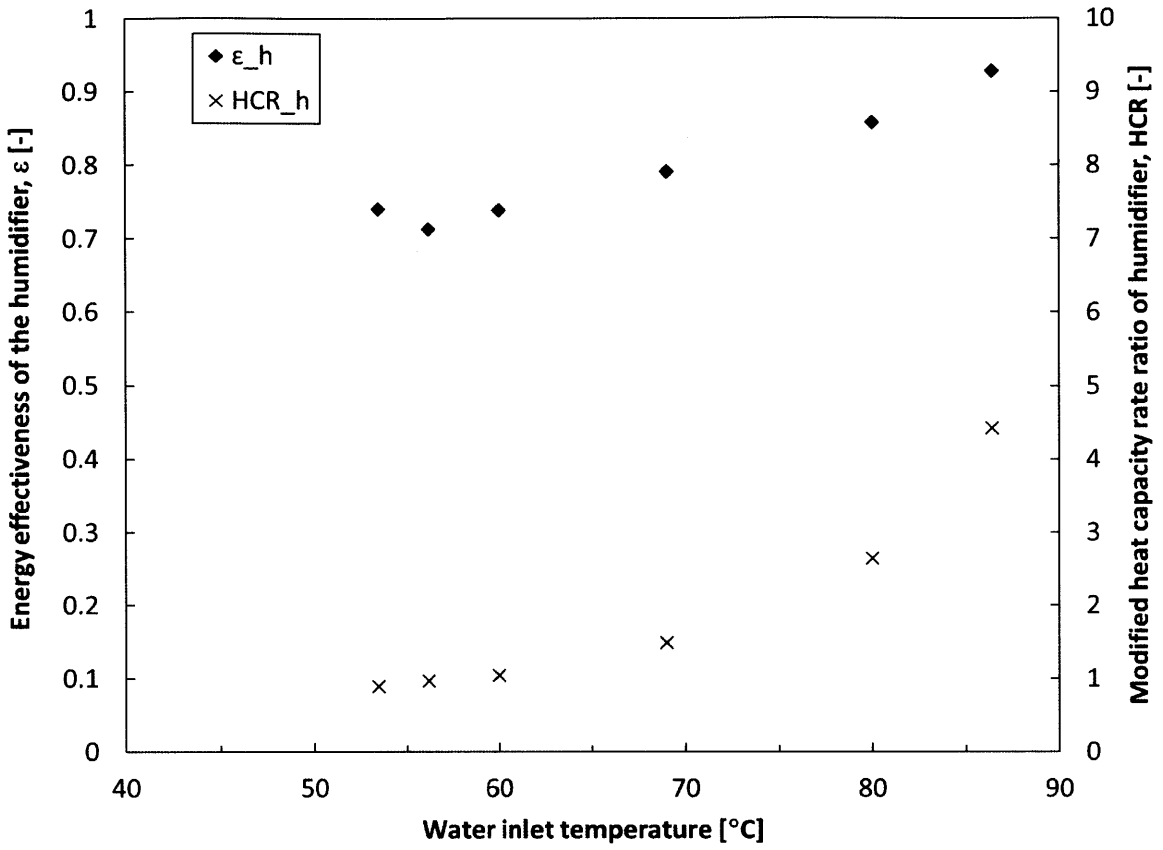

Figure 4-1: Water Inlet Temperature vs. Energy Effectiveness and Modified Heat Capacity Rate Ratio

It was suggested earlier in section 3.4 that non-dimensional entropy generation for a HME would be minimized by a heat capacity rate ratio of 1. Via modified heat capacity rate ratio, Figure 4-2 shows the effect of water inlet temperature on entropy generation, for the same data represented in the previous figure. It can be clearly seen from the figure that, like effectiveness, entropy generation is minimized by a HCRh of 1.

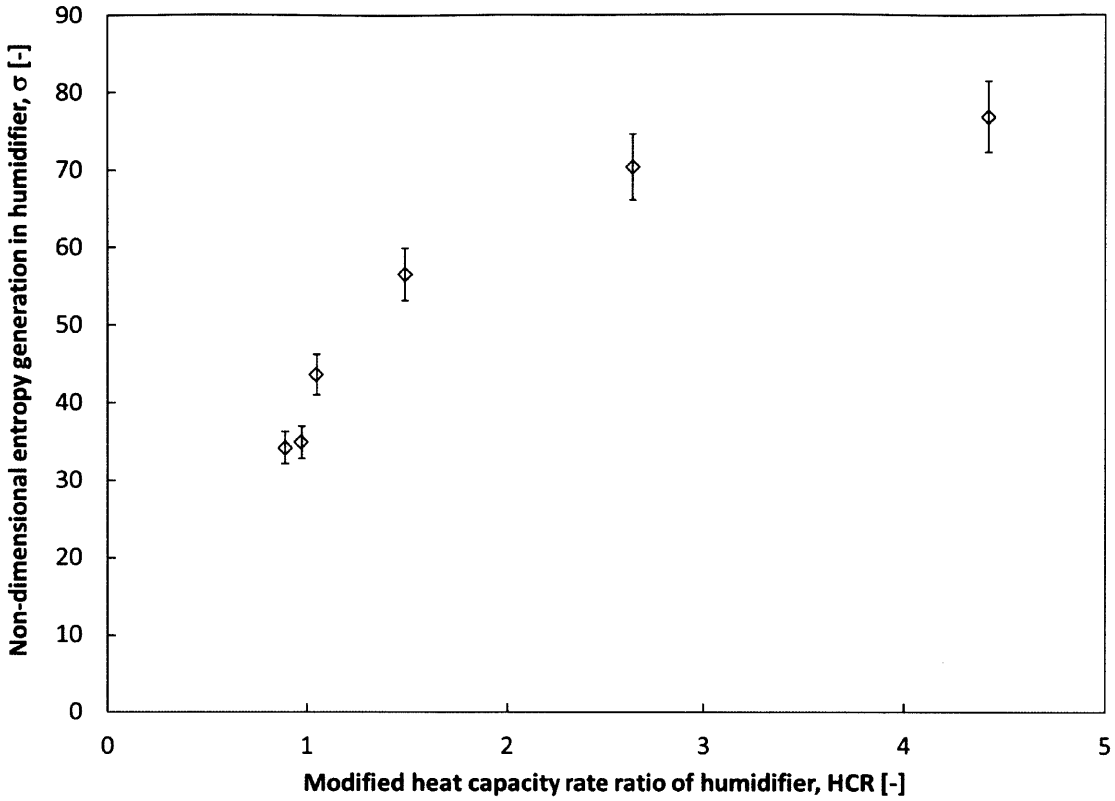

Figure 4-2: Modified Heat Capacity Rate Ratio vs. Non-Dimensional Entropy Generation for Varied Water Inlet Temperatures

4.2 Effect of Mass Flow Ratio

The effects on entropy generation of mass flow rate ratio are shown in Figure 4-3. For the data displayed here, mass flow rate ratio was varied by changing the flow rate of the water, fixing air flow rate at 16.52 standard liters per second. The water inlet temperature was fixed at 60 °C, and a fill volume of 4 blocks was used. While the graph only displays 4 data points, it is nonetheless apparent that there exists a local minimum near the mass flow rate ratio of 3.7. In the following graph, Figure 4-4, it can be seen that this apparent minimum corresponds to a HCRh of 1. Thus, with respect to flow rate variations as well as temperature variations, entropy generation

is minimized by a balanced heat capacity rate ratio.

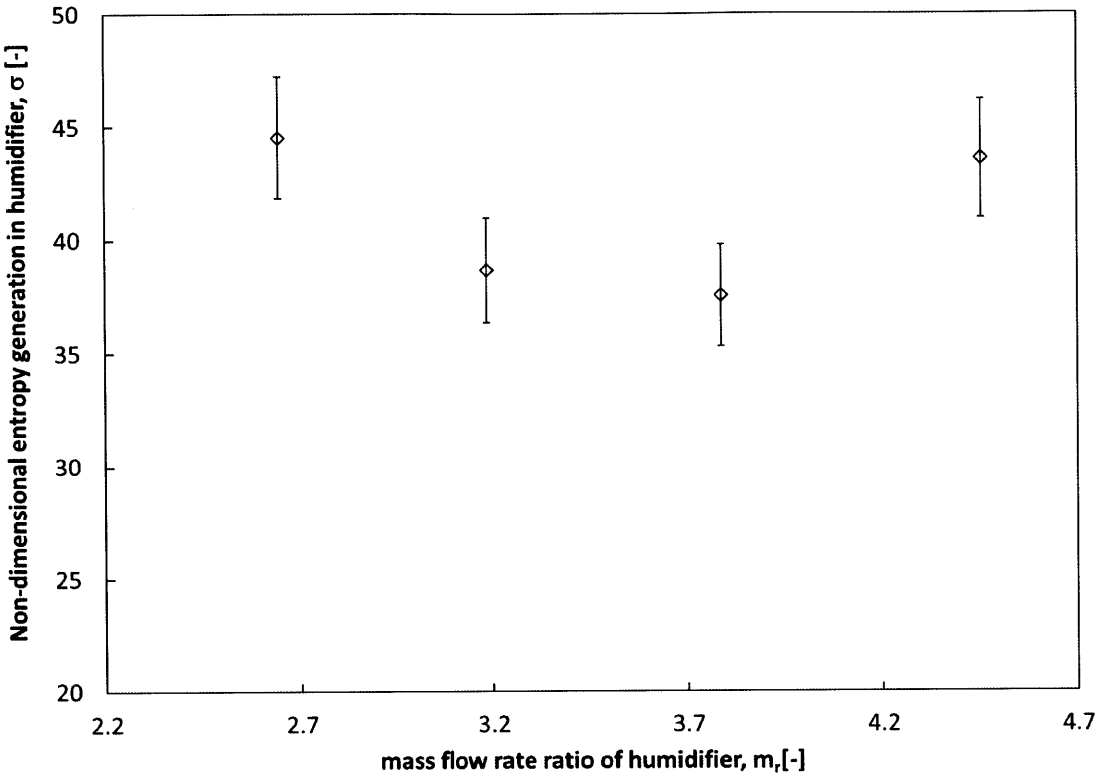

Figure 4-3: Mass Flow Rate Ratio vs. Non-Dimensional Entropy Generation

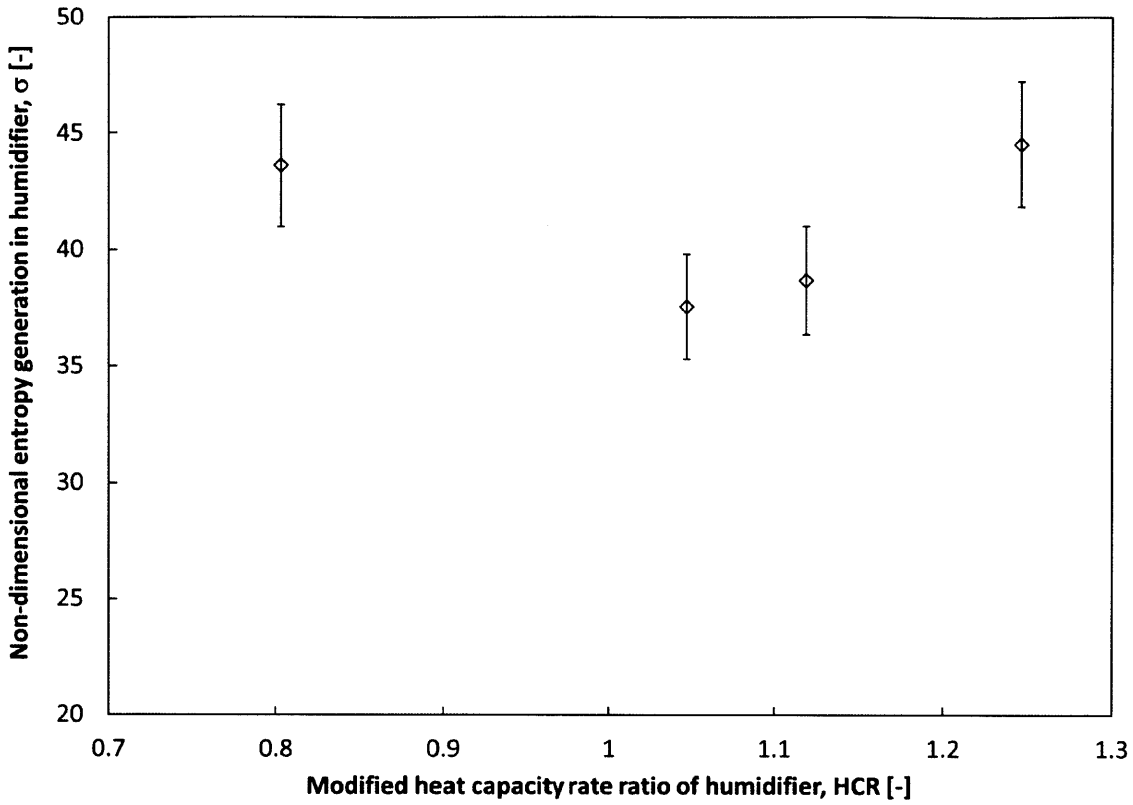

Figure 4-4: Modified Heat Capacity Rate Ratio vs. Non-Dimensional Entropy Generation for Varied Mass Flow Rate Ratio

4.3 Effect of fill volume

Figure 4-5 shows the energy effectiveness plotted against number of fill blocks used in the humidifier. For results presented in this figure, water inlet temperature was fixed at 60 °C, mass flow rate ratio at 2.9, and the amount of fill blocks in the humidifier was varied from 1 to 4. As explained in section 3.4, the outlet temperature of the lower heat capacity rate stream approaches the inlet temperature of the higher heat capacity rate stream as the size of the humidifier approaches infinity. Increasing the heat and mass transfer area of the humidifier by increasing the number of fill blocks inside brings the terminal temperature differences of the two

flows closer to 0, and increases the change in enthalpy rates of the two streams toward the infinite case. This conclusions is justified by Figure 4-5, which clearly demonstrates effectiveness as an increasing function of fill volume.

For the same set of results, 4-6 plots fill volume against enthalpy pinch. In the humidifier, air and water flows each have only one entry and one exit, so the volume between these points can be represented with a single control volume. Thus, enthalpy pinch is purely a function of end-conditions, so Figures 4-5 and 4-6 illustrate the same relationship. In both graphs, it can be seen that there are only marginal improvements after 4 blocks. This suggests that effectiveness and enthalpy pinch approach a limit where the water outlet temperature nears the air inlet temperature, at these fill volumes.

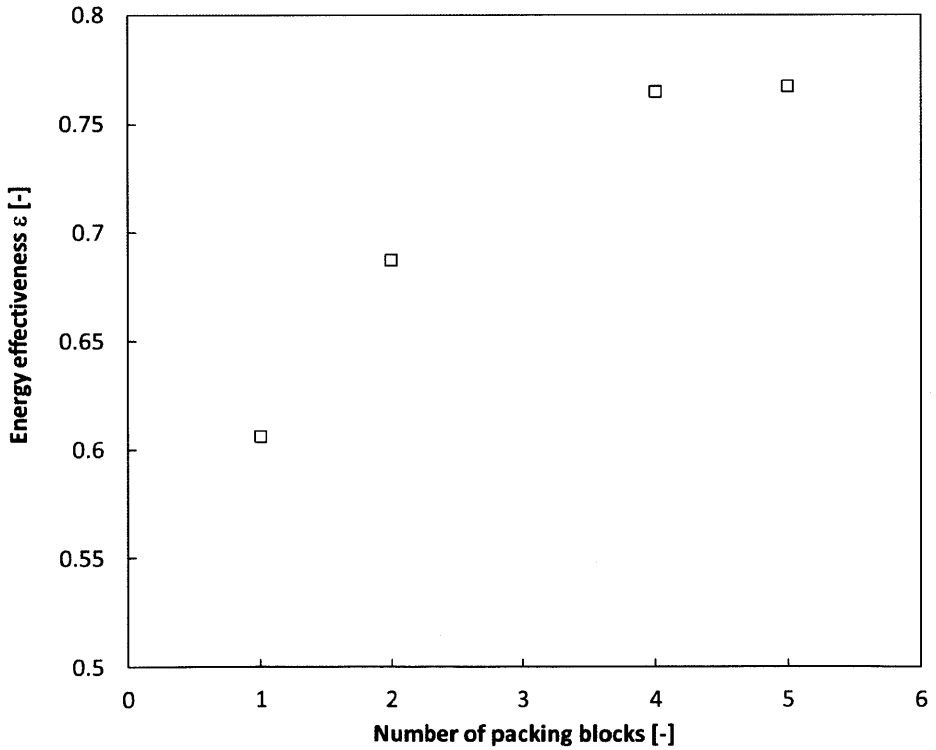

Figure 4-5: Number of Heat Transfer Fill Blocks in the Humidifier vs. Energy effectiveness.

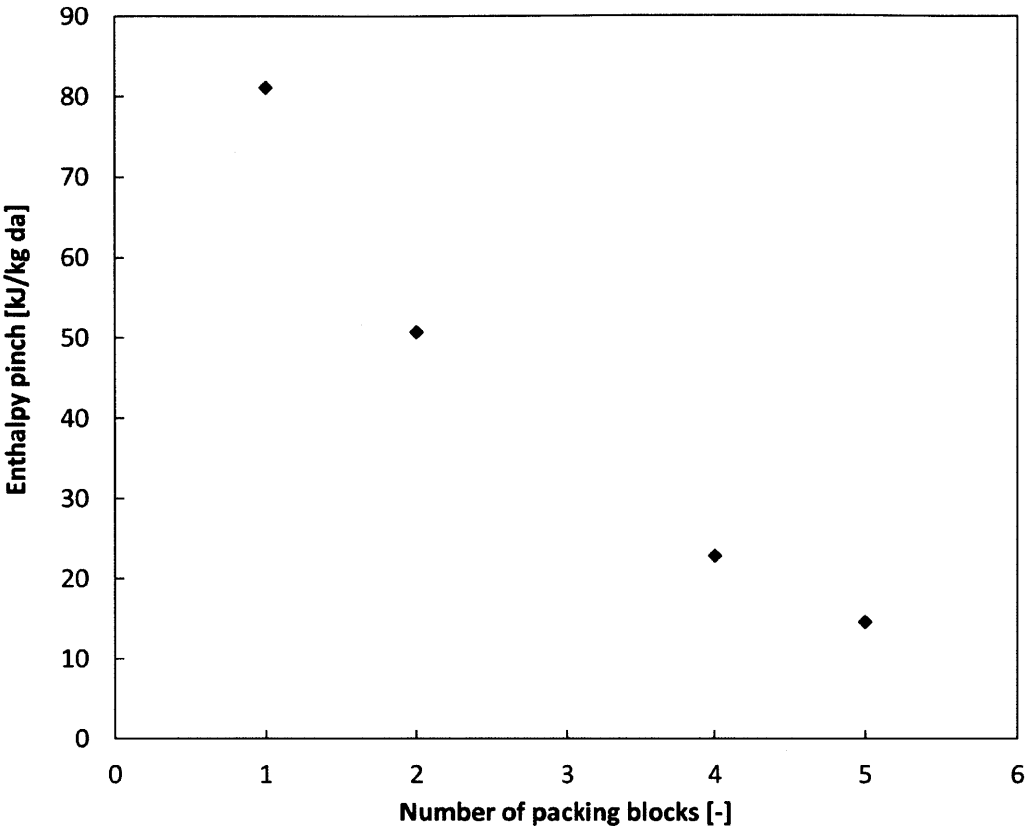

Figure 4-6: Number of Heat Transfer Fill Blocks in the Humidifier vs. Enthalpy Pinch

4.4 Temperature Profiles For Air and Water Flows at Optimal Performance

Figure 4-7 shows extrapolated temperature profiles for the air and water based on terminal temperatures measured for a HCR of 1 and 5 fills. This represents the optimized performance of the humidifier via balancing. The temperature pinch for these conditions is 2.8 °C, and the enthalpy pinch is 14.8 kJ/kg dry air.

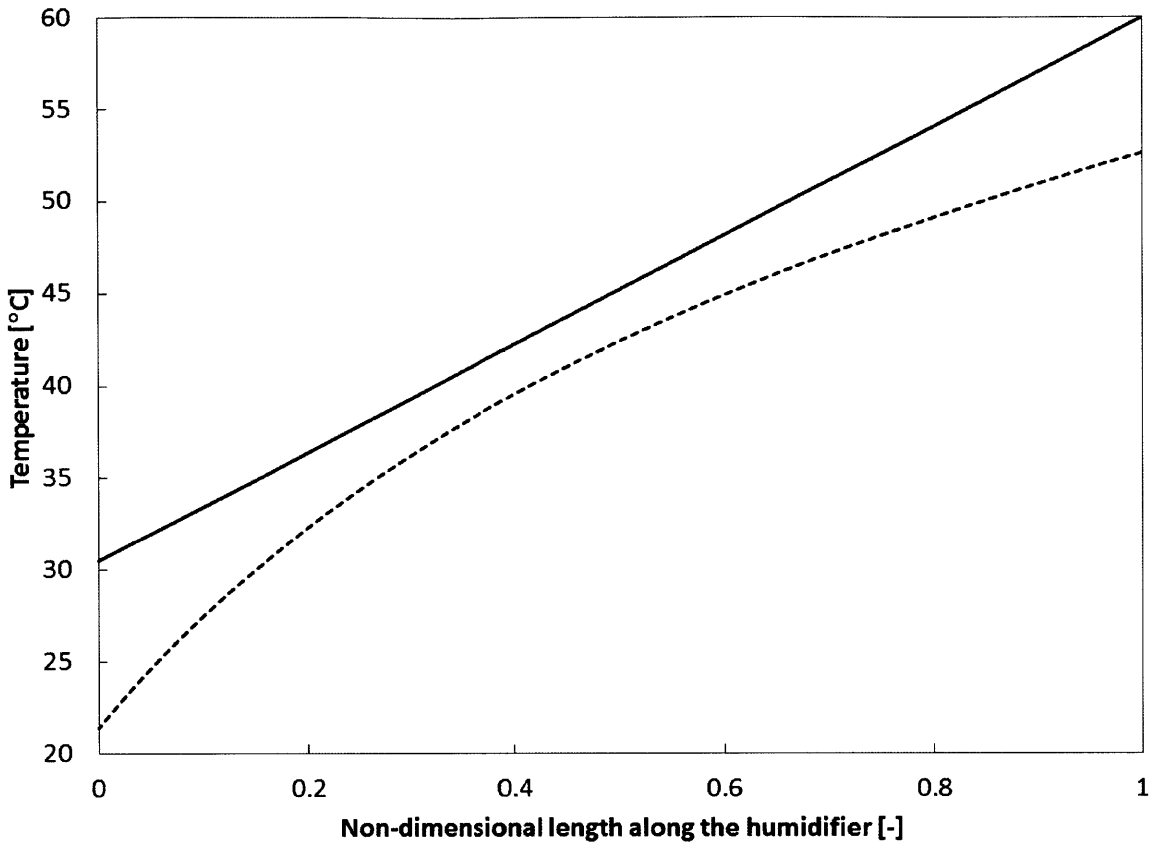

Figure 4-7: Temperature Profiles of Air and Water Flows for Balanced Heat Capacity Rate Ratio

5. Conclusions

The severity of water scarcity together with the widespread consumption of contaminated water in developing countries account for one of the greatest global health problems. Two billion people around the world do not have access to a reliable source of potable water. Water treatement via desalination techniques is a prospective solution to both scarcity and consumption problems. 98% of deaths caused by water related illnesses occur in the developing world. Lack of infrastructure and capital investment make small-scale local water treatment the most effective application of desalination technology in these places. The low capital cost, and competitive efficiencies of HDH make it the best suited technology for facilities like these.

1. An HDH plant featuring a packed bed humidifier was designed and built. The optimization point of the humidifier in terms of enthalpy pinch, non-dimensional entropy generation and effectiveness was demonstrated to coincide with balanced heat capacity flow ratios, validating the concept of thermal balancing for heat and mass transfer devices.

2. At these conditions, the humidifier had an effectiveness of 0.77, an enthalpy pinch of 14.8 kJ/kg, and a temperature pinch of 2.8 °C.

3. The theoretical framework for heat capacity rate ratio balancing establishes a design optimization technique that can be extended to HDH systems featuring mass extraction between the humidifier and dehumidifiers. Mass extractions allow systematic balancing of both the humidifier and dehumidifiers, which can allow for even greater water production efficiencies.

Bibliography

[1] Engelman, R., People in the Balance. Washington, D.C.: Population Action International, 2000. <www.populationaction.org>.

[2] Vigotti, R., Hoffman, A., Workshop on Renewable Energy and Water. IEA Working Party on Renewable Energy Technologies, 2009.

[3] Gardener-Outlaw, T., Engelman, R., Sustaining Water, Easing Scarcity: A Second Update. Washington, D.C.: Population International, 1997. <http://www.populationaction.org/Publications/Reports/Sustaining_Water_Easing_Scarcity/Sustaining_Water_Easing_Scarcity_-_Full_Report.pdf>.

[4] Clean Water: International Child Care, Inc. 2009. Accessed 20 May 2012. <http://www.intlchildcare.org/haiti_health_water.php>.

[5] Water.org. Accessed 24 May 2012. <http://www.water.org>

[6] Fawell, J., Bailey, K., Chilton, J., Dahi, E., Fewtrell, L., and Magara, Y., Fluoride in Drinking-Water. *WHO Drinking-water Quality Series*. London: IWA Publishing, 2008

[7] Schaaf, B., International Action's Campaign for Clean Water in Haiti. 1 Dec. 2008. Accessed 20 May 2012. <http://www.haitiinnovation.org/en/2008/12/02/international-actions-campaign-clean-water-haiti>.

[8] Guy, S., Haiti: The Struggle for Water. Frontline World. October 2004. Accessed 20 May 2012.<http://www.pbs.org/frontlineworld/fellows/haiti/indexb.html>.

[9] World Resources Institute 2003. Accessed 20 May 2012. <http://www.wri.org/>.

[10] Liburd, S.O., 2008. Solar-Driven Humidification Dehumidification Desalination for Potable Use in Haiti. Master's thesis, MIT, 2010

[11] Tomlinson, S, Desalination Plant Will Turn Seawater from the Thames Estuary into Drinking Water for One Million People as Drought Hits, *Daily Mail*, March 12, 2012, http://www.dailymail.co.uk/

[12] Miller, J., Review of Water Resources and Desalination Technologies. New Mexico: Sandia National Laboratories, 2003.

[13] Narayan, G., Sharqawy, M., Lienhard V, J., Zubair, S., and Antar, M., The potential of solar-driven humidification-dehumidification desalination for small-scale decentralized water production. Renewable and Sustainable Energy Reviews 14 (4), 1187-1201, 2010.

[14] Narayan, G.P., McGovern, R.K., Zubair, S.M. and Lienhard V, J.H., 2012. Continuous extraction in an infinitely large humidification dehumidification desalination system for attaining complete thermodynamic reversibility in water production, In Proceedings of Conference and Exhibition on desalination for the environment clean water and energy,

European Desalination Society, April 22-26, 2012, Barcelona, Spain.

[15] Georg Fischer LLC, GF Calorplast Heat Exchanger Brochure. 2009. Accessed May 20, 2012

[16] Georg Fischer LLC. Accessed May 20, 2012. <http://www.us.piping.georgefischer.com> [image sources only]

[17] Narayan, G.P., Sharqawy, M.H., Lam, S., Das, S. K. and Lienhard V, J.H., 2012. Bubble columns for condensation at high concentrations of non-condensable gas: heat transfer model and experiments, AIChE Journal, under review.

[18] Sharqawy, M.H., Lienhard V, J.H., Zubair, S.M. On Thermal Performance of Seawater Cooling Towers. Proceedings of the International Heat Transfer Conference. IHTC14, 23200, International Heat Transfer Conference, Washington DC, USA, 2010.

[19] Narayan, G.P., personal communication. July 13, 2011.

[20] Gast Manufacturing, Inc. Accessed May 21, 2012. <http://www.gastmfg.com/>

[21] Taco, Inc. Accessed May 21, 2012. <http://www.taco-hvac.com> [imaged edited to exclude other pump data]

[22] Huang, J., 2012. Design of a Mobile Community Level Water Treatment System Based on Humidification Dehumidification Desalination. Undergraduate thesis, MIT, 2012

[23] Kays, W.M., London, A.L.. Compact Heat Exchangers, McGraw-Hill, New York, 1st Edition, 1958

[24] Lienhard IV, J.H., and Lienhard V, J.H. A Heat Transfer Textbook. Cambridge: Plogiston Press, 2008

[25] Narayan, G.P., Lienhard V, J.H, and S.M. Zubair, 2010. Entropy generation minimization of combined heat and mass transfer devices. International Journal of Thermal Sciences, 49 (10), pp. 2057-2066.

[26] Narayan, G.P., Chehayeb, K.M., McGovern, R.K., Thiel, G.P., Zubair, S.M., Lienhard V, J.H., 2012. Thermodynamic balancing of the humidification dehumidification desalination system by mass extraction and injection, under review.

[27] Narayan, G.P., Sharqawy, M.H., Lienhard V, J.H., Thermodynamic Analysis of Humidification Dehumidification Desalination Cycles, Desalination and Water Treatment, 16 (2010), pp. 339-353